Available online at www.sciencedirect.com
SCIENCE DIRECT®
Journal of Sound and Vibration 278 (2004) 807–823
JOURNAL OF SOUND AND VIBRATION
www.elsevier.com/locate/jsvi

Anisotropy in the sound field generated by a bubble chain

Richard Manasseh[a,*,1], Aneta Nikolovska[b], Andrew Ooi[b], Shizuo Yoshida[c]

[a] *Energy and Thermofluids Engineering, CSIRO Manufacturing & Infrastructure Technology, P.O. Box 56, Highett, VIC 3190, Melbourne, Australia*

[b] *Department of Mechanical & Manufacturing Engineering, University of Melbourne, VIC 3010, Melbourne, Australia*

[c] *Laboratory of Physical Fluid Dynamics, Graduate School of Engineering, Hokkaido University, North 13 West 8, Sapporo 060, Japan*

Received 6 May 2003; accepted 16 October 2003

Abstract

A vertical chain of rising bubbles represents a transition from individual to continuum behaviour in a compressible gas–liquid flow. Experiments on the distribution of acoustic pressure around a bubble chain revealed a strong anisotropy in the acoustic field in the frequency band generated by individual bubbles. Sound appeared to propagate much more efficiently along the chain than normal to it. A simple theoretical model using a linear coupled-oscillator approximation was developed to explain this result. Although comparison with experiments is inherently qualitative, the model clearly demonstrated the anisotropy. The model also reproduced the change in pulse waveform along the chain. The results suggest that the enhancement of sound intensity along the chain can to some extent be explained by bubbles acting as resonant amplifiers re-transmitting vibrations.

1. Introduction

Sounds emitted by bubbles have been studied quantitatively since the time of Rayleigh [1]. A good review of bubble acoustics was made by Leighton [2]. Bubbles produce an acoustic signal owing to compression of the gas in the bubble. The 'spring' of the compressible gas and the mass of liquid around the bubble create a natural oscillator, sending a pressure fluctuation through the liquid. For a bubble detaching from a parent body of gas, the initial compression or rarefaction of the gas may be caused by the recoil of the bubble neck on formation, or by deformation of the

*Corresponding author. Tel.: +61-392-526-340; fax: +61-392-526-252.
E-mail address: richard.manasseh@csiro.au (R. Manasseh).
[1] CSIRO: Commonwealth Scientific and Industrial Research Organisation.

0022-460X/$ - see front matter
doi:10.1016/j.jsv.2003.10.015

bubble during its motion, although the mechanism of either process is still the subject of research [3,4]. Under adiabatic conditions, the natural frequency of a single, millimetre-sized, linearly oscillating bubble is given by [5]

$$\omega_0 = \sqrt{\frac{3\gamma P_0}{\rho R_0^2}}, \tag{1}$$

where ω_0 is the radian frequency, γ is the ratio of specific heats, P_0 is the absolute liquid pressure, ρ is the liquid density and R_0 is the equivalent spherical radius of the bubble. The Minnaert equation (1) is a simplified solution to the general equation for spherical bubble oscillations usually called the Rayleigh–Plesset equation [2]. A 6 mm diameter bubble, such as the ones studied here, has a natural frequency of about 1 kHz.

The acoustic behaviour of pairs of bubbles, mostly under the influence of an applied sound field, has been the subject of significant research (e.g. Refs. [6–11]). Much of this work is directed to predicting the relative motion of pairs of acoustically driven bubbles.

The acoustics of clouds or 'swarms' of bubbles, where the number of bubbles is large enough for the ensemble to be treated by a continuum approximation, has likewise been extensively researched (e.g. Refs. [12–16]).

The fluid dynamics of a single chain of rising bubbles has been studied by several authors (e.g. Refs. [17,18]), without considering its acoustics. As the number of bubbles in the chain becomes large, and certainly once multiple chains are introduced side-by-side, the system becomes more like a 'cloud' than a 'chain'. In the limit of large numbers of bubbles, a continuum acoustic theory (e.g. Ref. [15]) should become valid.

Considering briefly the continuum limit, a small quantity of gas has a dramatic influence on the 'averaged' speed of sound of the medium. It is easy to show that when the void fraction reaches 50%, the speed of sound c_m of an 'averaged' medium drops to only 25 m s^{-1}, lower than the speed of sound in air. A laboratory tank inevitably places top and bottom boundaries on a bubble cloud, permitting wave modes of the entire cloud with wavelengths λ on the order of the tank height. Although individual millimetre-sized bubbles have acoustic frequencies in the order of 1000 Hz, a bounded 'averaged-medium' cloud in a tank a quarter-metre high would have frequencies of its lower modes in the order of c_m/λ, which could be as low as 100 Hz. Thus, when there are a very large number of bubbles in a laboratory tank, an anisotropy in the sound field at frequencies of order 100 Hz should be expected. Such an anisotropy would correspond to the mode structure of the bounded cloud and was clearly demonstrated by Nicholas et al. [15]. However, the sound distribution around a chain of a finite number of bubbles has not been studied.

The acoustic behaviour of a bubble chain is of particular interest for feedback measurements of industrial aerators [19–21] and for the emission of sound by submarines [22].

This paper investigates a transition from individual bubble-acoustic behaviour to continuum behaviour, using a single chain of bubbles as the paradigm. Frequencies in the bandwidth of the individual bubble resonances, of order 1000 Hz, were investigated. Experiments presented in Section 2 demonstrate an anisotropic sound distribution for a low number of bubbles in a chain, at frequencies around 1000 Hz. In Sections 3 and 4 a simple coupled-oscillator model is developed

to try to explain the data from the experiment. In Section 5 the model and experiment are compared and contrasted.

2. Experiments

The experimental set-up is shown in Fig. 1. A chain of air bubbles was produced in water by a highly repeatable system similar to that of Manasseh et al. [4]. The number of bubbles in the chain was varied systematically. Further details are in Ref. [23]. The nozzle had a 5.000 ± 0.025 mm internal orifice diameter; it was supplied with air via a precision pressure regulator (CompAir Maxam type A216) at about 13.0 kPa pressure. Small variations of about ± 0.5 kPa were sufficient to establish steady and repeatably different bubble production rates. The nozzle was machined to maintain its edge as sharp as possible; this ensured a known contact radius for the forming bubbles. The nozzle orifice used for bubble production was 0.55 m below the water surface. The typical appearance of the bottom of the chain is shown in Fig. 2.

No external acoustic forcing was applied. The newly formed bubble at the base of the chain emitted a pulse of sound as it detached [4]. Such pulses die off over 10–20 ms, whereas the time interval between the bubble-formations creating the pulses was more than 50 ms.

A fixed hydrophone (Fig. 1) detecting the pulse from the newly formed bubble (the generator of the sound) triggered signal acquisition from a traversing hydrophone, ensuring the same pulse initiated signal acquisition in both near and far fields. The signal from the fixed hydrophone was used as the trigger because the signal near the nozzle is highly repeatable under these conditions [4]. Pairs of such keyed pulse waveforms from several points in a vertical plane were recorded.

Initial tests determined the optimal dimensions of the tank. The sound of a single bubble was measured in different-sized rectangular and cylindrical tanks. For very small tanks (0.1 m or less

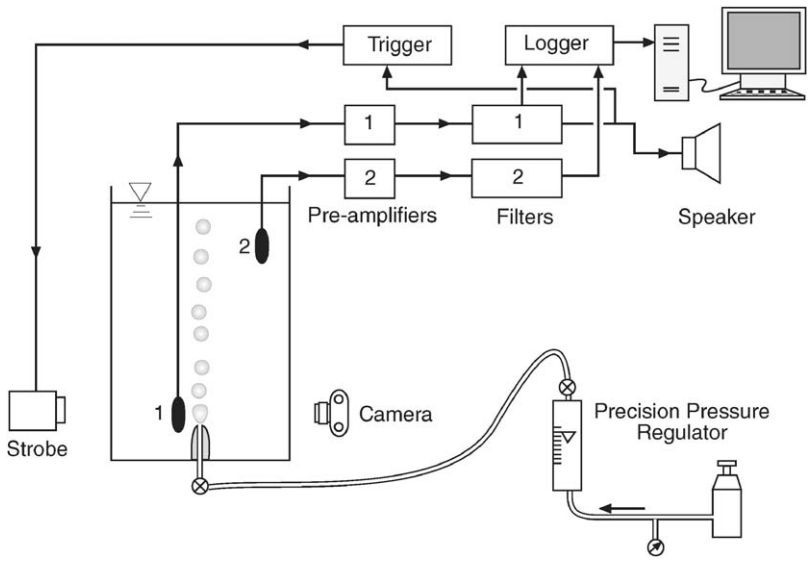

Fig. 1. Schematic of the experimental set-up. (1) fixed hydrophone and (2) traversing hydrophone.

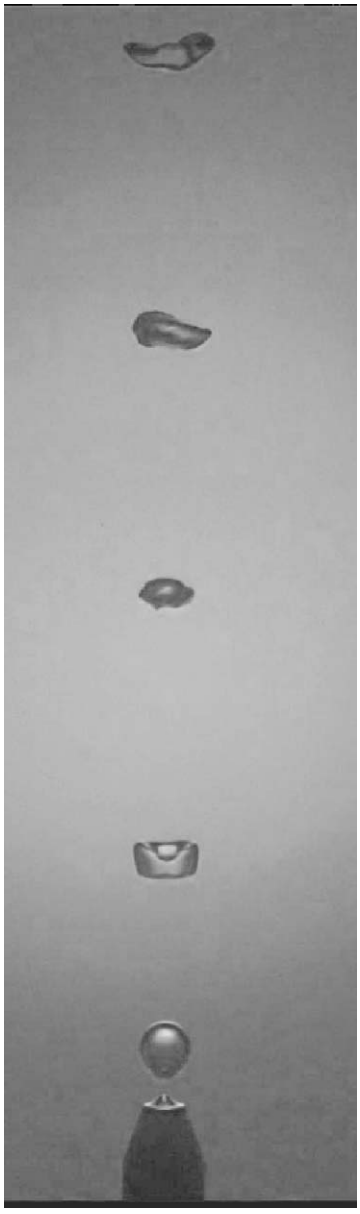

Fig. 2. Bubble chain at 8 Hz production rate.

in horizontal dimension) the size of the tank clearly influences the signal; and cylindrical-section tanks can significantly distort the signal, perhaps owing to focusing. A rectangular tank with negligible influence on the sound signal was selected. It was 0.88 m $\times$ 0.33 m in plane and 0.65 m deep. This tank was large enough for the results to appear independent of tank size, and tests in an even larger tank confirmed this. However, the only way to eliminate any influence of the tank walls is to make measurements in an unbounded domain; such experiments are currently planned.

Brüel & Kjaer type 8103 hydrophones were used for the fixed and traversing measurements. At the frequencies studied, this hydrophone type has an essentially spherical directivity field, ensuring sounds from any direction are equally transduced. The two hydrophone signals were pre-amplified by Brüel & Kjaer type 2635 charge amplifiers set to the individual calibrations of the hydrophones. The signals were band-pass filtered between 3 Hz and 10 kHz by a Stanford Digital SR560 filter. Acoustic pressures were digitized as transduced voltage by a National Instruments Data Acquisition Card type 6024E using the StreamTone (TM) software, which is built on the National Instruments LabView platform.

The acoustic centre of the fixed hydrophone was at a horizontal distance of 60 mm from the nozzle axis and in the vertical it was level with the plane of the nozzle orifice. This position was maintained for all of the experiments while the bubble-production rate (BPR) was varied. The traversing hydrophone was positioned on a 7×6 grid (60 mm grid spacing) in the vertical plane containing the nozzle axis.

Several pulses, typically 30–40, were acquired from the hydrophones at each grid point. The data could then be averaged and re-combined in several different ways to give a picture of the acoustic field around the bubble chain [23].

The number of bubbles in the chain was varied from 1 to approximately 30 by varying the air pressure in the nozzle. This increases the airflow rate, thereby producing bubbles more rapidly. The bubbles also increase in size, but most of the additional volume flow is achieved by increases in BPR [24]. Since bubbles rise at approximately the same speed for the bubble size range generated [25], increases in BPR increase the number of bubbles in the chain. As air flow was increased, the amplitude of the sound pulse measured by the fixed hydrophone at each bubble's formation rose from 1 Pa for 0.5 Hz BPR to 16 Pa for 18 Hz BPR.

The size of the bubbles was measured acoustically with (1) using the first-period method (Manasseh, [26]) but also checked visually to ensure (1) gave a reasonable prediction. Bubble size increased from an equivalent spherical radius R_0 of 2.60 ± 0.11 mm for 0.5 Hz BPR, to 4.10 ± 0.12 mm for 18 Hz BPR. The spacing between adjacent bubble centres, s, was measured photographically. The average spacing decreased from 0.55 m for 0.5 Hz (effectively, a single bubble in the tank depth) to about 0.017 m (about 30 bubbles) for 18 Hz. Data were recorded for bubble production rates of 8, 10, 13, 16 and 18 Hz.

A single bubble in the present experiment produces the classic 'impulse-response' exponentially decaying oscillation observed by experimentalists since Minnaert [5]. The oscillation amplitude decays from a maximum occurring in the first acoustic cycle or so. As the number of bubbles in the chain increases from one, interesting variations appear in the shape of the pulse, and these are quite repeatable up to the BPR where bubbles begin to pair [27]. Waveforms of typical pulses at the bottom of the chain are shown super-imposed in Fig. 3 to illustrate the repeatability of the experiment. The data are for 41 non-consecutive pulses. Random variations 'smudging' the super-imposition appear only after 10 or more cycles. The same data are shown averaged together in Fig. 4. The peaks have been reduced owing to the averaging, but the form is the same. It can be seen that there is an initial 'spike' with the maximum occurring in the first cycle or so, then a rapid 'decay' with some modulation. At different BPR, the severity of the decay or modulation can change. Nonetheless, at the bottom of the chain, there is always the same basic 'impulse-response' appearance.

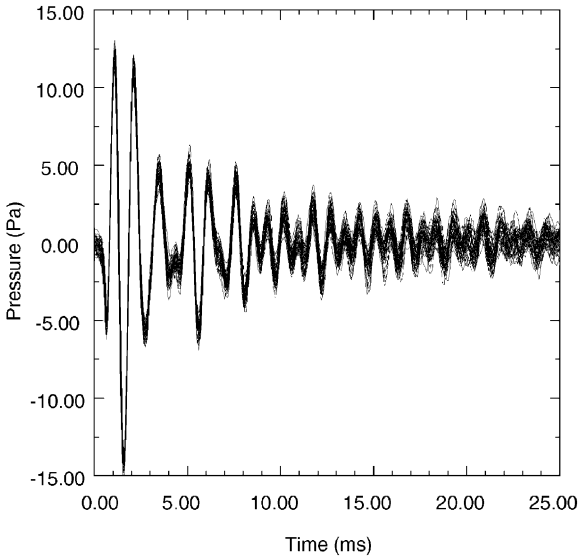

Fig. 3. Experimental pressure pulses at bottom of the chain (nozzle orifice depth) at 8 Hz BPR. Super-imposition of 41 pulses.

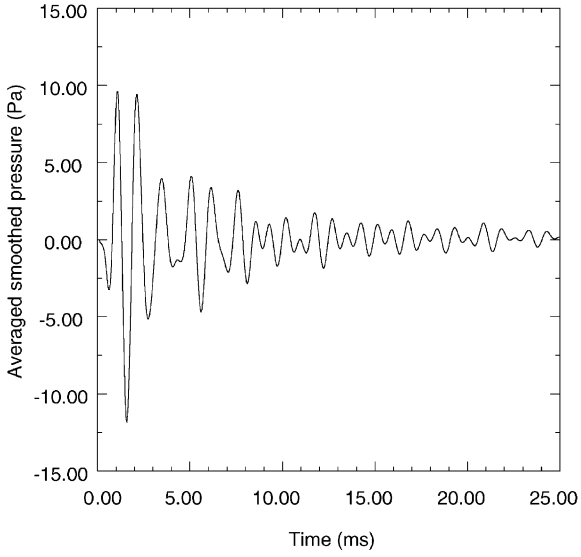

Fig. 4. Experimental pressure pulse at bottom of the chain (nozzle orifice depth) at 8 Hz BPR. Average of 41 pulses.

There is an important contrast with the waveforms high up the chain, shown superimposed in Fig. 5 and averaged in Fig. 6. Here, the pulse amplitude builds up to a maximum over about half a dozen cycles, then gradually decays; and the waveform has the clear appearance of being modulated.

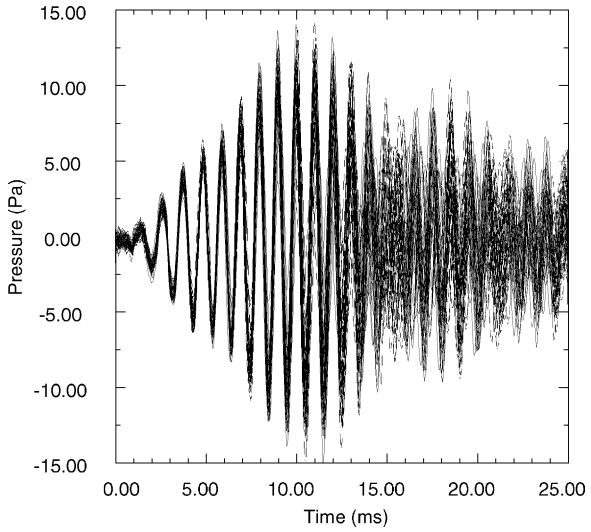

Fig. 5. Experimental pressure pulses at top of the chain (0.36 m above nozzle) at 8 Hz BPR. Super-imposition of 41 pulses.

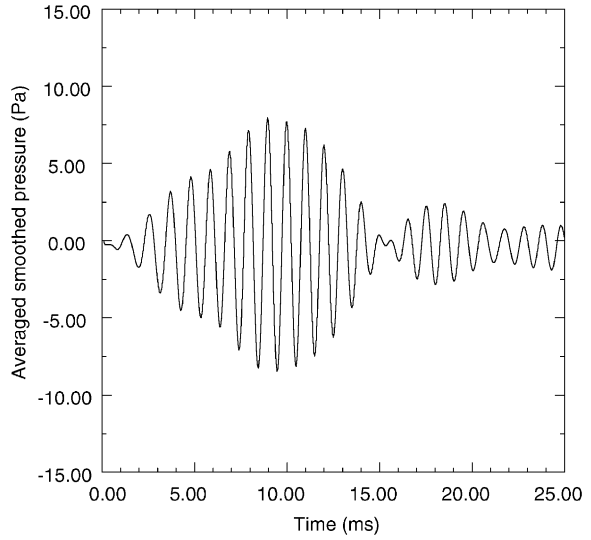

Fig. 6. Experimental pressure pulse at top of the chain (0.36 m above nozzle) at 8 Hz BPR. Average of 41 pulses.

The profiles of r.m.s. pressure ($P_{r.m.s.}$) along horizontal and vertical lines are shown in Figs. 7 and 8, respectively. Each point is $P_{r.m.s.}$ calculated over 25 ms for each pulse, and averaged over the pulses from 30 to 40 non-consecutive bubbles. The vertical profile of $P_{r.m.s.}$ clearly shows much higher intensities up the chain than the same distance horizontally away. The equivalent horizontal and vertical profiles for a single bubble appeared identical within the measurement

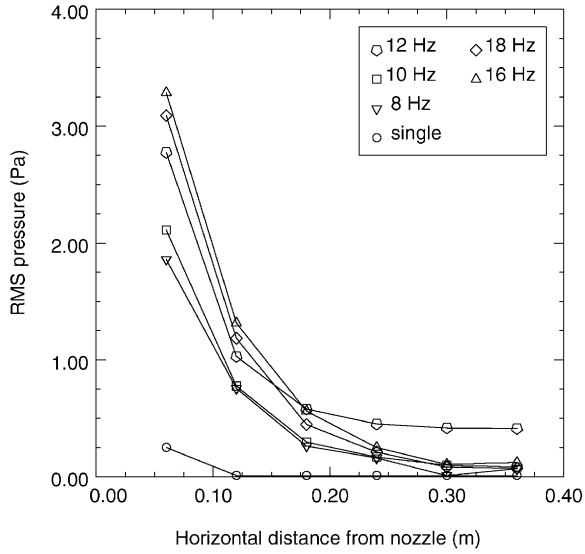

Fig. 7. Experimental radial $P_{r.m.s.}$ along a horizontal line at the nozzle depth. Profiles are for 8, 10, 13, 16 and 18 Hz BPR. Each point is average of $P_{r.m.s.}$ for 30–40 bubbles. Single-bubble $P_{r.m.s.}$ were calculated over 9 ms, exaggerating their relative magnitude, whereas all other $P_{r.m.s.}$ were calculated over 25 ms.

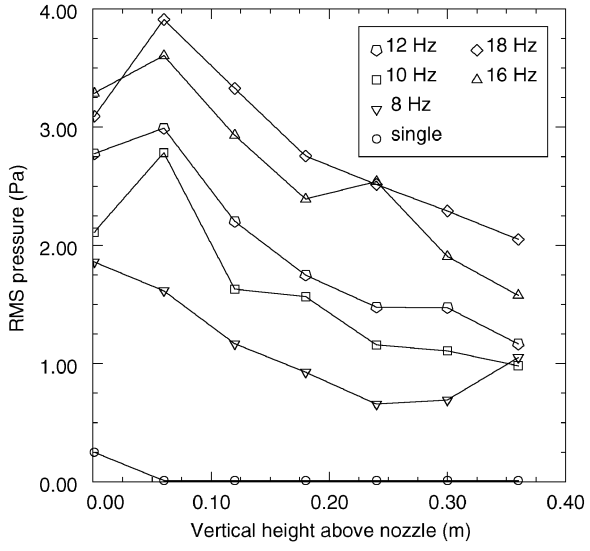

Fig. 8. Experimental vertical $P_{r.m.s.}$ along a vertical line 0.06 m from the nozzle axis. Profiles are for 8, 10, 13, 16 and 18 Hz BPR. Each point is average of $P_{r.m.s.}$ for 30–40 bubbles. Single-bubble $P_{r.m.s.}$ were calculated over 9 ms, exaggerating their relative magnitude, whereas all other $P_{r.m.s.}$ were calculated over 25 ms.

errors. Thus, the acoustic field around a bubble chain can be described as anisotropic, and the effect increases as bubble production rate increases. Although $P_{r.m.s.}$ does fall off with vertical distance from the source, the drop in the vertical is much less than that over the equivalent distance in the horizontal. This will be discussed in Section 5.

The vertical profile shows a significant separation between the profiles for different bubble production rates, with $P_{r.m.s.}$ increasing for higher BPR. This increase with BPR is also present in the horizontal profile, but is not so great.

In tests where the bubbles were formed near the tank centre, so sound could be measured below the bottom of the chain, the sound fell off very rapidly with vertical distance *below* the nozzle.

3. Coupled-oscillator theory

3.1. Formulation

The bubbles are assumed to lie on the z-axis of an axisymmetric cylindrical co-ordinate system (r, z) with z pointing downwards from the free surface. This assumption creates a fundamental inconsistency in co-ordinate systems, since the bubbles are assumed to be spherically symmetric (monopole) oscillators, while generating motions in the cylindrical frame. Provided the bubbles do not get too close, the inconsistency can be tolerated. As a consequence, this coupled-oscillator model, like some predecessors (e.g. Refs. [7,11]), cannot be considered mathematically rigorous. Analyses that could be combined to make a more thorough model are detailed elsewhere (e.g. Refs. [3,28,29]). Following straightforward derivations, the equations actually used in the present model for an arbitrary number of bubbles in a chain turn out similarly to those used previously for pairs of bubbles. In fact, any coupled mass–spring system is represented by similar equations.

Typical assumptions for millimetre-sized bubbles are that the gas is ideal with polytropic index κ; and that surface tension and vapour pressure effects are negligible. Then the gas pressure inside the ith bubble, $P_{Gi}(t)$, is simply given by $P_{Gi} = P_{0i}(R_{0i}/R_i)^{3\kappa}$ where R_{0i} is the equilibrium radius of the bubble, $R_i(t)$ is its time-dependent radius, and the absolute pressure including the hydrostatic head, P_{0i}, is given by $P_{0i} = P_{atm} + \rho g d_i$, where d_i is each bubble's depth. The pressure in the liquid just outside the bubble, $p_i(t)$, is assumed to be given by

$$p_i = P_{Gi} - \beta_i \dot{R}_i + \sum_{j \neq i} p'_j \frac{R_{0j}}{s_{ji}}, \tag{2}$$

where the spacing between the centres of bubbles i and j is denoted s_{ji}, the damping is represented by β_i, and the sum $p'_j(R_{0j}/s_{ji})$ accounts for the pressure perturbations p'_j of all the other bubbles, monopole in form and linearly superposed. The perturbations are given by

$$p'_i = P_{Gi} - \beta_i \dot{R}_i - P_{0i}.$$

A small-amplitude assumption, $R_i(t) = R_{0i} - \delta_i(t)$, $\delta_i \ll R_{0i}$, together with a small-velocity assumption, linearizes the Navier–Stokes equation for the liquid motion between neighbouring bubbles. Making consistent assumptions gives an approximate damping term B_i, given by $B_i = (4\eta/R_{0i}) + (\rho\omega_{0i}^2/c)R_{0i}^2$, where η is the liquid dynamic viscosity, ω_{0i} is given by Eq. (1) and c is the speed of sound in the liquid.

The foregoing assumptions transform the Navier–Stokes equation for the liquid motion to a set of linearly coupled equations

$$\ddot{\delta}_i + b_i \dot{\delta}_i + \omega_{0i}^2 \delta_i = -\sum_{j \neq i} \frac{R_{0j}^2/R_{0i}}{s_{ji}} (\omega_{0j}^2 \delta_j + b_j \dot{\delta}_j), \tag{3}$$

where $b_i = B_i/(\rho R_0)$. For identically sized bubbles (3) becomes

$$\ddot{\delta}_i + b_i\dot{\delta}_i + \omega_{0i}^2\delta_i = -\sum_{j\neq i}\frac{R_0}{s_{ji}}(\omega_{0j}^2\delta_j + b_j\dot{\delta}_j). \tag{4}$$

These are the coupled-oscillator equations actually used in the model. It should be noted that the coupling in the present model is due to the monopole super-imposition of the pressures from the other bubbles. In contrast to some other models (e.g. Ref. [11]), in the present model there are no coupling terms arising from the velocity fields of neighbouring bubbles. These were eliminated once boundary conditions on the top and bottom of the chain were imposed.

3.2. Simple case of two bubbles

The effectiveness of the model can only ultimately be tested by comparison with experiment; however, some physical insight can be gained by considering a simple two-bubble case first. For a pair of identical bubbles at the same depth so they have the same resonant frequency ω_0 and damping b, (4) becomes

$$\ddot{\delta}_1 + b\dot{\delta}_1 + \omega_0^2\delta_1 = -\frac{R_0}{s}(\omega_0^2\delta_2 + b\dot{\delta}_2), \tag{5}$$

$$\ddot{\delta}_2 + b\dot{\delta}_2 + \omega_0^2\delta_2 = -\frac{R_0}{s}(\omega_0^2\delta_1 + b\dot{\delta}_1), \tag{6}$$

where s is the distance between the centres. Anticipating a solution in the form of two eigenmodes, defining new variables $\xi = \delta_1 - \delta_2$ and $\chi = \delta_1 + \delta_2$ and adding and subtracting (5) and (6) gives

$$\ddot{\xi} + \left(1 - \frac{R_0}{s}\right)b\dot{\xi} + \left(1 - \frac{R_0}{s}\right)\omega_0^2\xi = 0, \tag{7}$$

$$\ddot{\chi} + \left(1 + \frac{R_0}{s}\right)b\dot{\chi} + \left(1 + \frac{R_0}{s}\right)\omega_0^2\chi = 0. \tag{8}$$

The first, low-frequency eigenmode ξ has, in the absence of damping, a frequency $\sqrt{(1 - R_0/s)}\omega_0$, while the second, high-frequency mode χ resonates at $\sqrt{(1 + R_0/s)}\omega_0$.

Once the model has been simplified to this extent, it has the same basic form as any of the models already proposed for two coupled bubble oscillators (e.g. Ref. [11]). There are two modes with frequencies $a_1\omega_0$ and $a_2\omega_0$, where a_1 and a_2 depend on the spacing s/R_0. As $s/R_0 \to \infty$, the eigenfrequencies tend to ω_0 and as $s/R_0 \to O(1)$, the eigenfrequencies diverge. For example, Hsiao et al. [11] calculate that the two modes have inviscid frequencies $\omega_0/\sqrt{1 + R_0/s}$ and $\omega_0/\sqrt{1 - R_0/s}$. It is straightforward to show that the difference in functional form of the eigenfrequencies between the present model and Hsaio et al.'s model arises from the fundamental difference in assumptions, not from any details of the derivation. If inertia terms corresponding to the velocity fields are included in the present model, it results in exactly the same eigenfrequency relations that Hsaio et al. obtain for the simple two-bubble case.

It can be seen from (7) and (8) that the low-frequency eigenmode has lower damping than the high-frequency eigenmode. This is consistent with general physical intuition, where low-frequency oscillations generally survive longer. Moreover, it suggests that if bubbles in a chain were hit by some impulse that excited multiple modes, the resulting pulse would decay with a frequency that would change with time. The pulse frequency would get lower as the higher-frequency modes died off, leaving the lower ones. Beats between the modes should be expected, modulating the pulse amplitude. A fall in the pulse frequency with time and modulations to its amplitude were observed by Manasseh [26] for a chain of bubbles formed from a nozzle.

4. Numerical method, settings and issues

The experimental signals show interesting phenomena inherently observed in the time domain, such as the modulation of the pulse produced on bubble formation, its decay, and the variation in pulse waveform at different heights up the chain. Thus, it is of interest to make a comparison with the model's predictions in the time domain. A set of N eigenmodes from a linear solution to (4) would not be useful, since the initial condition of each mode would have to be known.

In reality, the physical impulse exciting the bubble chain is, from the experiments of Manasseh et al. [4] and Section 2, the formation of the bubble at the nozzle. A jet penetrating the newly detached bubble was thought to provide the actual impulse initiating the acoustic oscillation. Translating this physical, three-dimensional impulse into an initial condition for the model is not simple, since the actual bubble-wall velocity, radius or internal pressure perturbation due to the impulse have not yet been measured. Nonetheless it is thought a more realistic and expedient test of the model to represent the impulse as a perturbation to the newly formed bubble, rather than attempting to project the impulse onto the set of eigenmodes.

Therefore the model was evaluated by simply integrating the coupled Eq. (4) forward in time. Settings for the model are shown in Table 1. Bubble sizes were set to those measured in the experiment for the same BPR. All parameters such as liquid density and viscosity, atmospheric pressure, gas compressibility, etc., were set to correct physical values. The number of bubbles, N, was based on the actual number in the chain at each experimental BPR, which was measured from photographs such as Fig. 2.

A fixed-timestep fourth order Runge–Kutta scheme was used. The model was first tested by checking it reproduced the 'beating' frequency between the two modes predicted for the simple two-bubble system in Section 3.2.

Table 1
Settings for the model based on experimental data

Experimental BPR (Hz)	0.5	—	—	8	10	12	16	18
Number of bubbles	1	2	5	16	19	21	27	30
Separation (mm apart)	—	250.0	100.0	32.1	24.9	27.1	19.4	17.4
Bubble diameter (mm)	5.21	5.21	5.21	7.00	7.00	7.51	7.85	8.22
Perturbation (mm s^{-1})	4.00	4.00	4.00	15.0	15.0	16.1	16.8	17.6

The separation is between bubble centres. The two and five bubble cases were only done numerically.

An initial perturbation in velocity, radius or pressure was applied to the newly formed bubble only: the bubble at the bottom of the chain. Equivalent perturbations in velocity, radius or pressure gave equivalent results as expected; and the results presented below are for a perturbation in velocity. (In future experimental work, it is anticipated that velocity would be easier to measure, by Particle-Image Velocimetry for example.)

In the absence of experimental information, the velocity perturbation was chosen to give the same pressure perturbation peak measured in the experiment, at the same measurement location. This setting of the initial condition was only done for the single-bubble case and for one bubble production rate, the lowest (8 Hz). As the experimental bubble production rate was increased, the magnitude of the peak pressure increased. As noted in Section 2, this may be due to the bubbles becoming larger, but they may also suffer proportionally larger perturbations at higher BPR. For BPR greater than 8 Hz, the velocity perturbation for the model was simply increased in proportion to the bubble size. This ignored the possibility of proportionally larger perturbations at higher BPR and the consequences will be discussed in the next section.

In reality, the bubbles are not equally spaced along the chain (Fig. 2). In particular, the first two or three bubbles are slightly closer, probably because some time is required for them to accelerate to a terminal velocity. Furthermore, bubbles higher up the chain form a spiral trajectory, departing from the assumed linear chain. Even if bubbles remained in-line, transfers of momentum due to the bubble wakes would cause non-uniform spacings of bubbles [18]. For the model, the bubbles were assumed to be equally spaced at the average of the spacings measured experimentally for each production rate.

Bubbles several millimetres in diameter only appear spherical immediately after formation. Once they have risen a few diameters, they become quite distorted (Fig. 2). This will change their resonant frequency slightly [30]. This would have the effect of 'detuning' the coupled oscillators, a further complication also not treated by the present model.

5. Comparison of model and experiment

Figs. 9 and 10 show the coupled-oscillator model's prediction of the pressure that would be measured by a hydrophone placed at the bottom and top of the chain, respectively. The model measured pressure $p_m(t)$ is the sum of the pressures $p_i(t)$ in the liquid at each bubble wall, reduced according to the monopole assumption,

$$p_m = \sum_{i=1}^{N} p_i \frac{R_0}{\sqrt{r^2 + (z - d_i)^2}}, \tag{9}$$

where (r, z) is the measurement point of interest. Figs. 9 and 10 should be compared with Figs. 4 and 6, respectively, for the experiment. Given the numerous approximations discussed above in Sections 3 and 4, the time series could not be expected to match well. Nonetheless, the key features of each waveform are correctly predicted. At the bottom of the chain, there is an initial sudden spike, then a rapid drop in signal magnitude over the first few cycles, then a recovery in the form of a modulation. High up the chain, there is no sharp start to the pulse, rather a gradual buildup to a modulated signal. (The amplitude appears higher in the model simply because the model

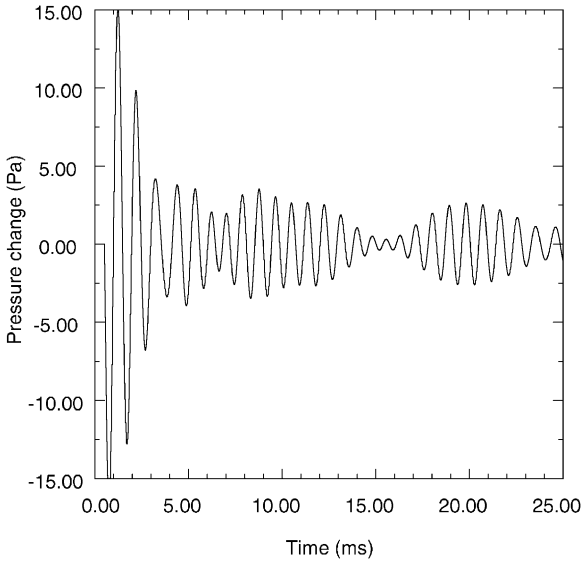

Fig. 9. Model pressure pulse p_m at bottom of the chain (nozzle orifice depth), for 8 Hz bubble production rate ($N = 16$).

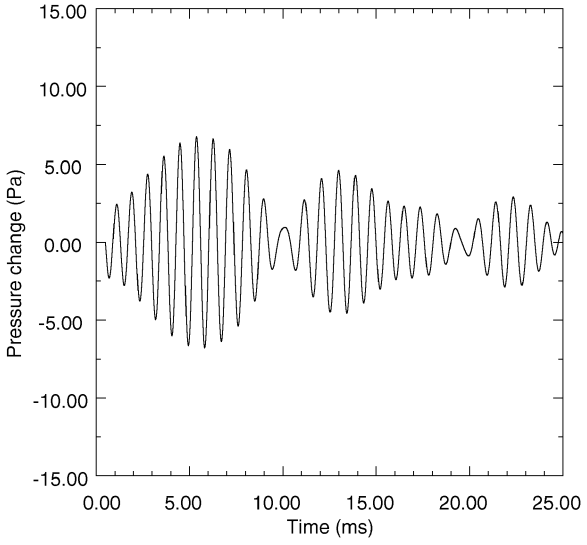

Fig. 10. Model pressure pulse p_m at top of the chain (0.36 m above nozzle), for 8 Hz bubble production rate ($N = 16$).

perturbation was set to reproduce the experimental peaks, and in Figs. 4 and 6 the peaks have been diminished by averaging—compare Figs. 9 and 3.)

The difference in signals can now be understood, particularly if the behaviour of the coupled-oscillator model is systematically studied as the number of bubbles is increased. Initially, only the newly formed bubble at the bottom is perturbed. However, all the other bubbles, while initially at

equilibrium, are 'hungry parasites'; ready to absorb energy from the perturbed bubble, since they have been initialized at the same size. The other bubbles in the model have almost the same resonant frequency, which differ only from the slight variations in P_0 due to their different depths. Hence, energy is rapidly absorbed from the newly formed bubble and re-distributed to the others. The result is that the pressure measured at the bottom, which is dominated by the pressure of the newly formed bubble, shows a rapid drop from the initial spike. The perturbation will excite a mixture of the N modes of the chain, which will interact causing a modulation as the modes beat against each other. Higher up the chain, the signal amplitude begins very low since the signal there is dominated by bubbles initially at equilibrium. Then, as the energy is transferred eventually to the topmost bubble, the signal envelope picks up with the modulation shown in Fig. 10.

The model's prediction of $P_{r.m.s.}$ is shown in Figs. 11 and 12. It can be seen that the vertical profile of r.m.s. pressure is quite level once there are more than $O(1)$ bubbles. In contrast, the horizontal profile decays in a $1/r$ manner as would be expected for a single bubble.

Thus, the model reproduced the same basic anisotropy as the experiment (Figs. 7 and 8). Notably, the experimental vertical profile of $P_{r.m.s.}$ does fall off with distance, whereas the model does not show this. The experimental drop in $P_{r.m.s.}$ in the vertical may be due to factors such as the shape-distortions of the bubbles and the spiralling and irregular behaviour which become more marked higher up the chain.

The transition from single-bubble to multiple-bubble behaviour can also be seen in Fig. 8. In addition to profiles for the number of bubbles in the experiment, profiles are plotted for one, two and five bubbles in the chain. For one, two and five bubbles, the perturbation was made equal so the profiles could be readily contrasted. The two-bubble profile shows an obvious 'bump' at the location of the second bubble, which picked up some energy from the newly formed bubble at the

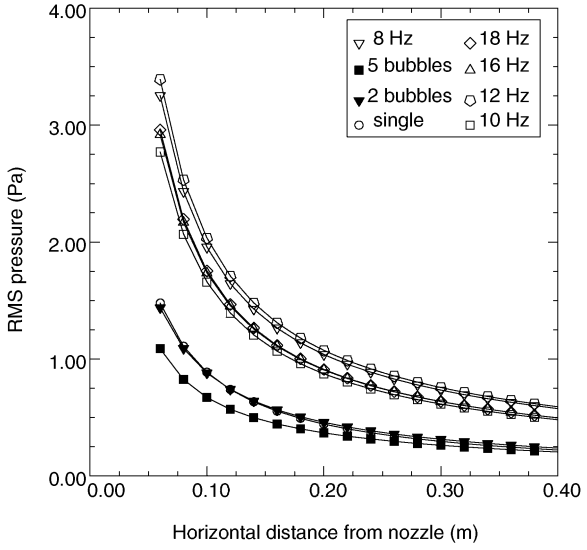

Fig. 11. Model radial r.m.s. pressure along a horizontal line at the nozzle depth. Profiles for 8, 10, 13, 16 and 18 Hz BPR are for perturbations proportional to experimental bubble radii. Single, two and five bubble profiles at the same perturbation as 8 Hz BPR.

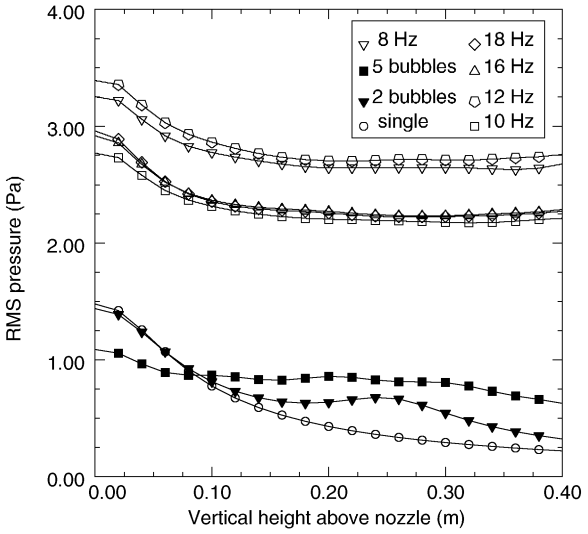

Fig. 12. Model vertical r.m.s. pressure along a vertical line 0.06 m from the nozzle axis. Profiles for 8, 10, 13, 16 and 18 Hz BPR are for perturbations proportional to experimental bubble radii. Single, two and five bubble profiles at the same perturbation as 8 Hz BPR; gradient discontinuity at $z = 0$ is because $P_{r.m.s.} \propto 1/\sqrt{(z^2 + (0.06)^2)}$, not $1/z^2$.

bottom. However, with five bubbles, the energy was distributed to four 'parasite' bubbles, and it is clear that the $P_{r.m.s.}$ in the vicinity of the newly formed bubble is significantly diminished as a consequence. Interestingly, the $P_{r.m.s.}$ profile for 8 Hz is higher than that for 10, 13 and 16 Hz. Examining the waveforms indicates a more rapid loss of amplitude for 10, 13 and 16 Hz, which resulted in a lower average pressure amplitude.

As noted in Section 2, the experimental vertical $P_{r.m.s.}$ profiles increase significantly with BPR. While this is also noticeable in the horizontal profiles, the effect is much more marked in the vertical profiles. This increase of the profiles is not found in model results, and in the case of the 8 Hz production rate the opposite trend was noted. Recalling that the model perturbations for 8–18 Hz BPR were simply set proportionally to the bubble size, this implies that in reality the perturbation increases more rapidly with BPR than the bubble size. By setting the model initial conditions appropriately, the shifts in experimental profiles could have been mimicked, but that would give a misleading impression of the model's capability. Overall, the experimental observation suggests that the anisotropy is enforced as BPR increases and brings bubbles closer together.

The experimental vertical $P_{r.m.s.}$ profiles show a peak at the second measurement height. This may be because in reality the initial perturbation, although generated by the newly formed bubble at the bottom, also initially excites the nearby bubbles.

6. Conclusion

Experiments on the distribution of acoustic pressure around a bubble chain revealed a strong anisotropy in the acoustic field. Sound appeared to propagate much more efficiently along the

chain than normal to it. The phenomenon was present in the resonant frequency band of individual bubbles. This may have relevance to the distribution of underwater sound generated by bubbles streaming from a vessel's hull or caught in its wake. It may also be relevant to the acoustic measurement and control of industrial bubbly flow systems, in which sound may be measured far from its source.

A simple theoretical model using a linear coupled-oscillator approximation of the chain was evaluated. The model qualitatively reproduced the change in pulse waveform along the chain. Most significantly, despite its simplifications, the model also qualitatively predicted the anisotropy in the acoustic field. However, the comparison remains qualitative, limited by ignorance on the true initial conditions in the experiment, as well as by the simplifications inherent in the model. The results suggest that the enhancement of sound intensity along the chain can to some extent be explained by bubbles acting as resonant amplifiers re-transmitting vibrations.

Future theoretical work should address the limit as the number of bubbles becomes large, possibly by using a continuum-based model. The coupled-oscillator model should be extended to include bubble rise velocities. Experiments or numerical simulations should be made to determine the true initial conditions of the newly formed bubbles. Experiments should also be made in an unbounded domain to assess the influence of walls.

Acknowledgements

We are grateful to Li Chen at the Australian Defence Science and Technology Organisation (DSTO) and John Davy, Anh Bui, Ian Shepherd and Frank LaFontaine at CSIRO for discussions, and to Lachlan Graham, Tony Swallow and Anthony Antzakas at CSIRO for help with the experiments. AN is supported by The University of Melbourne through MIRS and MIFRS grants (00-1456) and by DSTO/CSIRO through the SPS grant.

References

[1] Lord Rayleigh, On the pressure developed in a liquid during the collapse of a spherical cavity, *Philosophical Magazine* 34 (1917) 94–98.
[2] T.G. Leighton, *The Acoustic Bubble*, Academic Press, London, 1994.
[3] M.S. Longuet-Higgins, Monopole emission of sound by asymmetric bubble oscillations. Part 1. Normal modes, *Journal of Fluid Mechanics* 201 (1989) 525–541.
[4] R. Manasseh, S. Yoshida, M. Rudman, Bubble formation processes and bubble acoustic signals, *Proceedings of the Third International Conference on Multiphase Flow*, Lyon, France, 8–12 June, 1998.
[5] M. Minnaert, On musical air bubbles and the sound of running water, *Philosophical Magazine* 16 (1933) 235–248.
[6] V.F.K. Bjerknes, *Fields of Force*, Columbia University Press, New York, 1906.
[7] E.A. Zabolotskaya, Interaction of gas bubbles in a sound field, *Soviet Physics-Acoustics* 30 (1984) 365.
[8] H.N. Ogũz, A. Prosperetti, A generalization of the impulse and virial theorems with an application to bubble oscillations, *Journal of Fluid Mechanics* 218 (1990) 143–162.
[9] A.A. Doinikov, S.T. Zavtrak, On the mutual interaction of two gas bubbles in a sound field, *Physics of Fluids* 7 (8) (1995) 1923–1930.
[10] A. Harkin, T.J. Kaper, A. Nadim, Coupled pulsation and translation of two gas bubbles in a liquid, *Journal of Fluid Mechanics* 445 (2001) 377–411.

[11] P.-Y. Hsaio, M. Devaud, J.-C. Bacri, Acoustic coupling between two air bubbles in water, *European Physical Journal E* 4 (2001) 5–10.
[12] K.W. Commander, A. Prosperetti, Linear pressure waves in bubbly liquids: comparison between theory and experiments, *Journal of the Acoustical Society of America* 85 (2) (1989) 732–746.
[13] N.Q. Lu, A. Prosperetti, S.W. Yoon, Underwater noise emissions from bubble clouds, *IEEE Journal of Oceanic Engineering* 15 (4) (1990) 275–281.
[14] Z.W. Qian, Sound propagation in a medium containing bubbles and the splitting of the resonance peak, *Journal of Sound and Vibration* 168 (2) (1993) 327–337.
[15] M. Nicholas, R.A. Roy, L.A. Crum, H.N. Ogũz, A. Prosperetti, Sound emission by a laboratory bubble cloud, *Journal of the Acoustical Society of America* 95 (6) (1994) 3117–3182.
[16] M. Watanabe, A. Prosperetti, Shock waves in dilute bubbly liquids, *Journal of Fluid Mechanics* 274 (1994) 349–381.
[17] J.F. Harper, On bubbles rising in line at large reynolds numbers, *Journal of Fluid Mechanics* 41 (1970) 751–758.
[18] M.C. Ruzicka, On bubbles rising in line, *International Journal of Multiphase Flow* 26 (7) (2001) 1141–1181.
[19] J.W.R. Boyd, J. Varley, The uses of passive measurement of acoustic emissions from chemical engineering processes, *Chemical Engineering Science* 56 (2001) 1749–1767.
[20] R. Manasseh, R.F. LaFontaine, J. Davy, I.C. Shepherd, Y. Zhu, Passive acoustic bubble sizing in sparged systems, *Experiments in Fluids* 30 (6) (2001) 672–682.
[21] H. Chanson, R. Manasseh, Air entrainment processes of a circular plunging jet: void-fraction and acoustic measurements, *Journal of Fluids Engineering, Transactions of American Society of Mechanical Engineers* 125 (5) (2003) 910–921 (ISSN 0098–2202).
[22] L. Chen, R. Manasseh, A. Nikolovksa, C. Norwood, Noise generation by an underwater gas jet, *Proceedings of the Eighth Western Pacific Acoustics Conference*, Melbourne, Australia, 7–9 April, 2003.
[23] A. Nikolovksa, R. Manasseh, A. Ooi, Visualizing the acoustic field around a chain of bubbles using a hydrophone-scanning method, *Proceedings of the Seventh Asian Symposium on Visualisation*, Singapore, 26–30 May, 2003.
[24] R. Clift, J.R. Grace, M.E. Weber, *Bubbles, Drops and Particles*, Academic Press, London, 1978.
[25] T. Maxworthy, C. Gnann, M. Kürten, F. Durst, Experiments on the rise of air bubbles in clean viscous liquids, *Journal of Fluid Mechanics* 321 (1996) 421–441.
[26] R. Manasseh, Acoustic sizing of bubbles at moderate to high bubbling rates, in: M. Giot, F. Mayinger, G.P. Celata (Eds.), *Experimental Heat Transfer, Fluid Mechanics and Thermodynamics*, Edizioni ETS, Pisa, 1997, pp. 943–947.
[27] R. Manasseh, Bubble-pairing phenomena in sparging from vertical-axis nozzles, Vol. 5, *Proceedings*, *24th Australian & NZ Chemical Engineering Conference*, Sydney, 30 September–2 October, 1996, pp. 27–32.
[28] Z.C. Feng, L.G. Leal, On energy transfer in resonant bubble oscillations, *Physics of Fluids A* 5 (4) (1993) 826–836.
[29] G.L. Chahine, Bubble interactions with vortices, in: S. Green (Ed.), *Fluid vortices*, Kluwer Academic Publishers, Dordrecht, 1995, pp. 783–828.
[30] M. Strasberg, The pulsation frequency of nonspherical gas bubbles in liquid, *Journal of the Acoustical Society of America* 25 (3) (1953) 536–537.